Desalination and Water Treatment
www.deswater.com

doi: 10.5004/dwt.2023.29977

311 (2023) 188–195
November

Hydrothermal preparation of carbon adsorbent from 1,2-dichloroethane waste liquid assisted by nonylphenol ethoxylate

Xinying Yu, Wenqi Zhang*, Ziyun Yao, Jiawei Wang

College of Chemistry and Chemical Engineering, Shanghai University of Engineering Science, Shanghai, 201620, China, Tel. +86-159-0074-6789; Fax +86-021-6779-1214; email: zhangwenqi@sues.edu.cn (W. Zhang), Tel. +86-150-8246-1771; email: 2435280760@qq.com (X. Yu), Tel. +86-139-5688-6716; email: 1009023459@qq.com (Z. Yao), Tel. +86-188-6753-5969; email: 1849581780@qq.com (J. Wang)

Received 29 May 2023; Accepted 15 September 2023

ABSTRACT

Chlorinated organic pollutants have been recognized as one of the major problems in the field of environmental engineering. In this work, 1,2-dichloroethane (DCE) waste liquid was used as feedstock to produce carbon adsorbent through the hydrothermal carbonization process. And the effects of nonylphenol ethoxylate (NP-10)/DCE mixing ratio, sulfuric acid initial concentration, and reaction time on the adsorption capacity of hydrochars at 180°C were investigated. Properties of the NP-10/DCE blended hydrochars were assessed by scanning electron microscopy, Brunauer–Emmett–Teller, and Fourier-transform infrared spectroscopy analysis. Experimental results show that the hydrochar obtained by using 50% DCE and 50% NP-10 with 71 wt.% sulfuric acid at 5 h demonstrated the best surface area (567.61 $m^2 \cdot g^{-1}$) and abundant functional groups. The methylene blue adsorption experiments indicated that the maximum adsorption capacity of the hydrochar was 440.49 $mg \cdot g^{-1}$, which was higher than that of commercial activated carbon (261.74 $mg \cdot g^{-1}$). This study provides a novel approach for the disposal of chlorinated organic waste liquids.

Keywords: Hydrothermal carbonization; 1,2-Dichloroethane waste liquid; Nonylphenol ethoxylate; Carbon adsorbent

1. Introduction

Numerous chlorinated organic contaminants are toxicity and bioaccumulation and have been included in the list of the highly harmful chemicals targeted in most countries [1,2]. Several methods have been developed to treat chlorinated organic compounds, including adsorption [3–5], oxidation–reduction [6–9], biodegradation [10–12], and incineration [13–15]. Direct incineration has been one of the most effective means for disposing of high concentration chlorinated organic waste liquids and solid wastes for many years. However, this process could release toxic byproducts, such as dioxins and hydrochloric acid (HCl) [16]. Furthermore, from the aspect of energetic recovery efficiency, the heating value of many chlorinated organic compounds was low [17]. Therefore, it is vital to seek a safe and effective method for the resource utilization of chlorinated organic wastes.

In recent years, hydrothermal carbonization (HTC) technology has been widely applied as a new method for the disposal of chlorinated organic solid wastes. It has been demonstrated that solid fuel and functional carbon materials could be produced via the HTC of polyvinyl chloride (PVC) [18,19]. Moreover, the dechlorination effect and adsorption performance of hydrochars could be improved through co-hydrothermal carbonization of PVC with biomass waste such as bamboo, pomelo peel, and corncob [20–22]. However, the disposal of chlorinated organic waste liquids via the HTC process has not been reported.

* Corresponding author.

1,2-Dichloroethane (DCE) is one of the most popular organic solvents used in the chemical industry and the global production of DCE exceeds 15.8 million tons per year [23,24]. Thus, large amounts of DCE waste liquid (about 28% of global production) could be generated and need to be treated. In this work, HTC technology was adopted to dispose of DCE waste liquid. However, due to its low carbon content, DCE waste liquid must be disposed of other organic compounds through co-hydrothermal carbonization to improve the yield of hydrochar.

Nonylphenol ethoxylate is a typical non-ionic surfactant widely used in agricultural and industrial applications [25]. It has been demonstrated in our previous studies that carbon adsorbent could be produced from nonylphenol ethoxylate (NP-10) waste liquid via hydrothermal carbonization under acidic conditions [26]. And NP-10 can also effectively assist the hydrochar formation from phenolic waste liquid [27]. This study aims to prepare carbon adsorbent through the hydrothermal carbonization of DCE waste liquid with the assistance of NP-10.

2. Materials and methods

2.1. Materials

1,2-Dichloroethane (AR) and methylene blue ($C_{16}H_{18}ClN_3S{\cdot}3H_2O$) were purchased from Sinopharm Chemical Reagent Co., Ltd. The NP-10 waste liquid was supplied by a chemical enterprise in Zhejiang Province, China. The total solid (TS) of the waste liquid was measured to be 60 wt.% by the gravimetric method. Sulfuric acid (AR, 98%) and activated carbon (AR, 200 mesh) were purchased from Shanghai Titan Scientific Co., Ltd. Deionized water was produced by ultrapure water systems (Heal Force, Shanghai, China).

2.2. Hydrothermal carbonization experiment

The HTC experiments were performed in a 100 mL Teflon-lined miniature magnetic autoclave with a stainless-steel pressure gauge (Binhai, Jiangsu, China). The temperature of 180°C was selected because of the previous study of NP-10 HTC, and at this temperature condition, the pressure of the reactor was 1.7 MPa for the 40 wt.% DCE. To obtain hydrochar with excellent adsorption performance under more economical conditions, the experimental conditions of NP-10/DCE mixing ratio, sulfuric acid concentration, and reaction time were optimized. The reaction conditions and experimental results are shown in Table 1. The reactor was heated up to 180°C at a heating rate of 5°C/min. As the reaction time reached, the autoclave was cooled down to room temperature naturally. The hydrochar was washed with 200 mL of distilled water. Solid–liquid separation was achieved by filtering through a quantitative filter paper (medium speed). Then the hydrochar was dried in the oven at 80°C for 6 h, and stored in an air-tight plastic tube for subsequent characterization.

The yield of hydrochar was measured using an analytical balance and calculated according to Eq. (1).

$$Y(\%) = \frac{W_{hc}}{W_{fz}} \times 100 \tag{1}$$

where W_{hc} and W_{fz} represent the final weight of dry hydrochar and the weight of feedstocks (DCE and NP-10), respectively.

The consumption of acid (H_c) was calculated according to Eq. (2).

$$H_c = H_d - H_r \tag{2}$$

where H_c, H_d, and H_r represent the consumption of acid, initial dosage of acid, and acid residue in the washing water, respectively.

The acid residue and the chemical oxygen demand (COD) of the washing water were conducted by acid–base titration and potassium dichromate method, respectively, according to standard methods issued by the State Environmental Protection Administration of China (2002) [28].

Table 1
Sample names, conditions, chemical oxygen demand of washing water, acid consumption, yield, and adsorption quantity

Sample	Volume ratio of NP-10/DCE	Initial concentrations of sulfuric acid (wt.%)	Reaction time (h)	COD ($mg{\cdot}L^{-1}$)	Acid consumption (mmol)	Yield (%)	Q_e ($mg{\cdot}g^{-1}$)
S0D1	0:1	0	3	5,800	–	–	–
N0D1	0:1	78	3	344	27.16	0.84	–
N0.2D1	0.2:1	78	3	120	18.30	8.43	158
N0.5D1	0.5:1	78	3	192	25.94	11.72	194
N1D1	**1:1**	**78**	**3**	**304**	**35.32**	**16.29**	**266**
N2D1	2:1	78	3	320	75.48	21.60	240
S62T3	1:1	62	3	628	9.86	14.24	35
S67T3	1:1	67	3	514	14.13	16.28	90
S71T3	**1:1**	**71**	**3**	**312**	**20.83**	**16.28**	**257**
S87T3	1:1	87	3	228	48.43	16.38	287
S71T1	1:1	71	1	432	13.58	13.53	109
S71T5	**1:1**	**71**	**5**	**176**	**28.25**	**16.49**	**301**
S71T7	1:1	71	7	248	25.66	16.38	273

2.3. Characterization of hydrochars

The surface morphology and hydrochar structure were characterized by scanning electron microscopy (SEM) (Germany ZEISS Sigma 300) with an accelerating voltage of 5 kV, and before observation, the hydrochars were gold coated. Functional groups of hydrochar were investigated by Fourier-transform infrared spectroscopy (FTIR; Thermo Scientific Nicolet iS5, USA), and samples were scanned from 4,000 to 400 cm^{-1} with a resolution of 4 cm^{-1}. Nitrogen adsorption/desorption measurement was analyzed by using a gas sorption analyzer (Micromeritics ASAP 2460, USA), and the specific surface area was calculated by using the Brunauer–Emmett–Teller (BET) model.

2.4. Batch adsorption assays

The obtained carbon adsorbents were ground and screened by 200 mesh sieves. Kinetic adsorption experiments were performed at 25°C. A mass of 15 mg of the adsorbent was added to 500 mL of the methylene blue (MB) solution with 10 $mg{\cdot}L^{-1}$ initial concentration and kept in a shaker of 150 rpm. Samples were taken at a certain interval time, filtered through a 0.22 μm membrane, and analyzed using the UV-Vis spectrophotometer at its maximum wavelength of 664 nm (UV-5100, Shanghai Metash Instruments Co., Ltd.). The adsorption capacity at time t and at equilibrium, Q_t ($mg{\cdot}g^{-1}$) and Q_e ($mg{\cdot}g^{-1}$) were calculated by Eqs. (3) and (4), respectively [29].

$$q_t = \frac{\left(C_0 - C_t\right)V}{m} \tag{3}$$

$$q_e = \frac{\left(C_0 - C_e\right)V}{m} \tag{4}$$

where C_0 is the initial MB solutions concentration ($mg{\cdot}L^{-1}$), C_t and C_e are the concentration of dye at time t and equilibrium, respectively. m indicates the quality of the adsorbent (g) and V represents the volume of MB solutions (L).

The pseudo-first-order and pseudo-second-order kinetic models were adopted to analyze adsorption kinetics data [29]. The models were expressed as Eqs. (5) and (6), respectively.

$$\ln\left(Q_e - Q_t\right) = \ln Q_e - k_1 t \tag{5}$$

$$\frac{t}{Q_t} = \frac{1}{k_2 Q_e^2} + \frac{t}{Q_e} \tag{6}$$

where k_1 (min^{-1}) and k_2 ($g{\cdot}mg^{-1}{\cdot}min^{-1}$), respectively indicate the rate constants of pseudo-first-order and pseudo-second-order kinetic models, and t is the contact time (min).

The adsorption isotherm was conducted by adding 15 mg adsorbent to 500 mL solution with initial MB concentrations of 10, 15, 20, 25, 30, 35, 40, and 45 $mg{\cdot}L^{-1}$, respectively. The aqueous samples were taken and filtered to determine the C_e when the adsorption equilibrium was reached. The adsorption isotherm data was calculated by Langmuir and Freundlich models [29]. The models were expressed as Eqs. (7) and (8), respectively.

$$Q_e = \frac{Q_m K_L C_e}{1 + K_L C_e} \tag{7}$$

$$Q_e = K_F \times C_e^{1/n} \tag{8}$$

where Q_m ($mg{\cdot}g^{-1}$) is the maximum adsorption capacity, and K_L ($L{\cdot}mg^{-1}$) is the constant. K_F ($L{\cdot}g^{-1}$) and n are Freundlich constants that give a measure of adsorption capacity and adsorption intensity, respectively.

3. Results and discussion

3.1. Optimization of HTC conditions

As shown in Table 1, in the absence of sulfuric acid for S0D1, the carbonization of DCE was incomplete under the conditions of 180°C at 3 h. The COD of the washing water was up to 5,800 $mg{\cdot}L^{-1}$, and from the GC-MS analysis (QP-2010, Ultra, USA), the main organic compounds in the washing water were DCE (65.86%), 2-chloroethanol (14.48%) and 1,4-dioxane (11.43%). However, the COD of the washing water for N0D1 was 344 $mg{\cdot}L^{-1}$ and no DCE was detected in GC-MS analysis, which evidenced that the addition of sulfuric acid could effectively promote the hydrothermal carbonization of DCE. Even so, due to the significantly low yield of 0.84%, the addition of NP-10 was necessary.

According to Table 1, it can be seen that under the condition of 78 wt.% sulfuric acid at 3 h, the yields of hydrochar, the COD of washing water, and acid consumption exhibited an increasing trend with the dosage of NP-10 increased from 0.2 to 2 mL. However, compared to N0D1 and N0.2D1, the addition of 0.2 mL of NP-10 results in a decrease in the COD of washing water, suggesting that NP-10 could enhance the carbonization degree of DCE. Moreover, compared the adsorption performance of the hydrochars (N0.2D1, N0.5D1, N1D1, N2D1) for MB, it was observed that the hydrochar obtained at an NP-10/DCE volume ratio of 1:1 exhibited the highest adsorption quantity.

Based on the optimum mixing ratio, the initial sulfuric acid concentration was further optimized. It is worth noting that when the sulfuric acid concentration was lower than 71 wt.%, the COD of washing water sharply increased and the adsorption performance significantly decreased. Specifically, the COD of washing water increased from 312 $mg{\cdot}L^{-1}$ of S71T3 to 514 $mg{\cdot}L^{-1}$ of S67T3, while the adsorption quantity of hydrochar decreased from 257 to 90 $mg{\cdot}g^{-1}$. This could be related to the difference in carbonization degree. With the initial sulfuric acid concentration exceeding 71 wt.%, the COD of washing water, yields of hydrochar, and the adsorption performance changed slightly, while the acid consumption raised significantly. To obtain hydrochar with excellent adsorption performance under more economical conditions, the concentration of sulfuric acid was optimized to 71 wt.%.

Furthermore, optimization of the reaction times was conducted. With the increase of reaction time in the range of 1–5 h, the MB uptake amount increased gradually from 109 to 301 $mg{\cdot}g^{-1}$, and the COD of the washing water decreased, corresponding to the acid consumption increased. When the reaction time was further prolonged to 7 h, compared to S71T5 and S71T7, the MB uptake amount and the

yield of hydrochar decreased slightly, inferring the hydrochar structure underwent some degree of alteration in the later stage of HTC. To further investigate the properties of hydrothermal carbon obtained under different reaction times, a series of subsequent analyses were conducted.

3.2. SEM analysis

Fig. 1 shows the SEM images of the hydrochars obtained at different reaction times. Two types of morphologies, the dense carbon spheres and the agglomerated particles can be observed in each sample (Fig. 1a–d). As shown, the diameter of dense carbon spheres was about 2–5 μm, which possessed a marginal impact on the pore volume and specific surface area of the hydrochar [30]. Generally, these textural properties of hydrochar were primarily influenced by the agglomerated particles. According to Fig. 1a, the small particles are tightly bonded to each other and formed densely packed granular protrusions (about 100 nm), which had a negative effect on well-developed pore structure.

When the reaction time was increased, especially at 5 h, the diameter of particles on the surface of the agglomerate decreased to about 20 nm, and a rich nano-scale pore structure formed (Fig. 1b–d). It can be inferred that the continuous dissolution and growth of the small particles led to the condensation polymerization and adjustment of the agglomerated particles in this process, which was in accordance with the Ostwald ripening theory [31,32]. Moreover, with the increasing reaction time, due to the escapes of HCl and carbon dioxide from the dichlorination and decarboxylation, plenty of pore structure in the hydrochar could also be formed [33,34]. However, when the reaction time was extended to 7 h, the pore structure exhibited minimal variation.

The SEM-energy-dispersive X-ray spectroscopy technique in Fig. 2 reveals the element proportions of hydrochars obtained at different reaction times. The chlorine content in the hydrochars gradually increased with the prolongation of the reaction time. The sulfur content in the hydrochars obtained at reaction times of 3–7 h showed a positive correlation with the consumption of sulfuric acid. However, the hydrochar obtained at 1 h exhibited the highest sulfur content, which may be attributed to its higher sulfuric acid concentration in the initial stage. As shown in Fig. 2b, with the reaction time increased from 1 to 3 h, both carbon and oxygen content increased. Upon further prolonging the reaction time, the variation of oxygen content exhibited a similar trend to that of sulfur content, which can be attributed to the variations in the sulfur-oxygen-containing functional groups of the hydrochar.

3.3. Surface area and pores analysis

Fig. 3a presents the nitrogen adsorption–desorption isotherms of hydrochars prepared in different reaction times. The isotherm of S71T1 fits the type-II sorption behavior according to the classification of gas adsorption isotherms, indicating the low level of adsorption capacities [35]. The S71T3, S71T5, and S71T7 exhibited a typical type-IV sorption isotherms with an obvious type-H4 hysteresis loop, which was usually attributed to adsorption occurring within micropores or mesopores [36]. This was supported by the range of the average pore size of 3–5 nm (Fig. 3b).

The specific surface area, pore volume, and pore size of hydrochar were estimated by the BET equation and the Barrett–Joyner–Halenda model (Table 2). At 1 h, the specific surface area of the hydrochar was merely 4.2 $m^2 \cdot g^{-1}$. As the reaction time extended to 3 h, the BET surface area

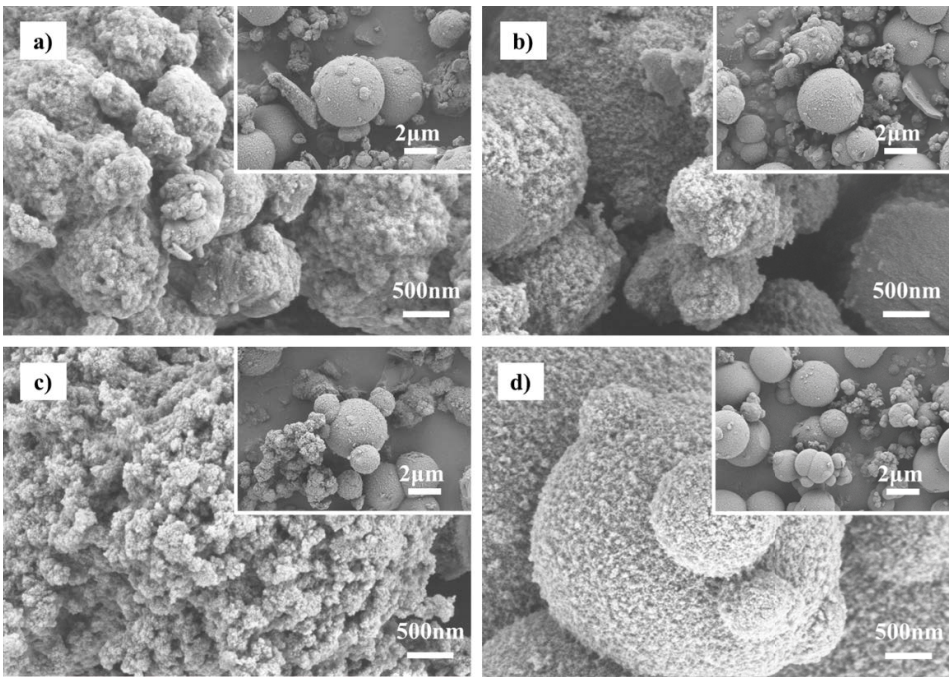

Fig. 1. Scanning electron micrographs of (a) S71T1, (b) S71T3, (c) S71T5, and (d) S71T7.

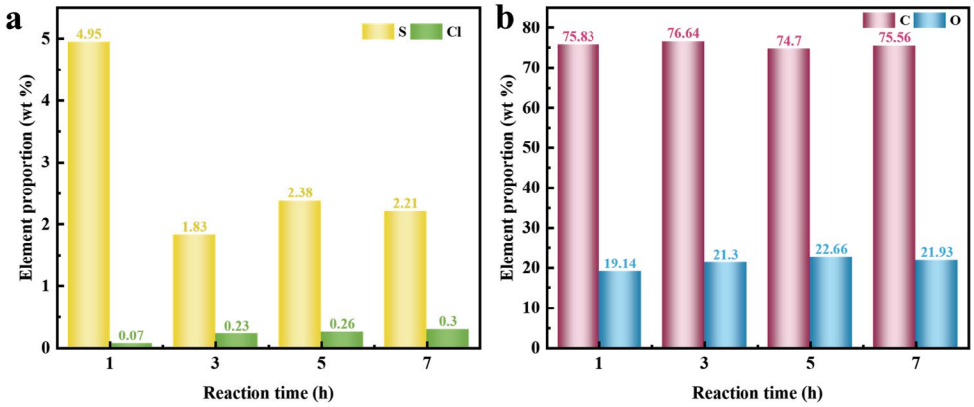

Fig. 2. Energy-dispersive X-ray spectroscopy mappings of hydrochars at various reaction times.

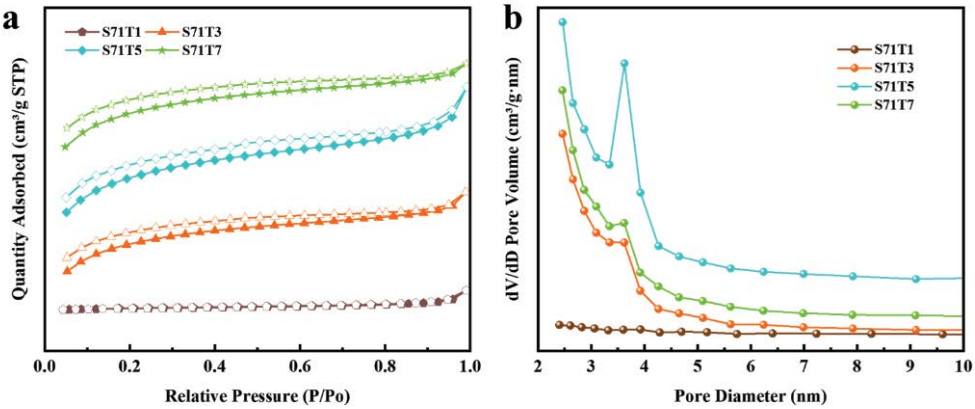

Fig. 3. (a) Nitrogen adsorption–desorption isotherms of hydrochars and (b) pore-size distribution calculated by Barrett–Joyner–Halenda of hydrochars.

Table 2
Specific surface area, total pore volume, and Barrett–Joyner–Halenda pore diameter of hydrochars prepared under difference reaction times

Sample	Specific surface area ($m^2 \cdot g^{-1}$)	Total pore volume ($cm^3 \cdot g^{-1}$)	Barrett–Joyner–Halenda pore diameter (nm)
S71T1	4.25	0.011	13.67
S71T3	492.90	0.018	3.72
S71T5	567.61	0.032	4.23
S71T7	532.80	0.019	3.64

correspondingly increased to 493 $m^2 \cdot g^{-1}$. With prolonging the reaction time to 5 h, the BET surface area continued to rise and peaked at 568 $m^2 \cdot g^{-1}$. However, when the reaction time extended to 7 h, the BET surface area showed a slight decline, supposing that part of the holes collapsed or covered after a longer time under this condition.

3.4. FTIR analysis

As shown in Fig. 4, the hydrochars obtained in this study exhibited a broad variety of functional groups compared to the commercial activated carbon (AC). The peak observed around 3,700–3,200 cm^{-1} corresponded to the stretching vibrations of –OH and –COOH, indicating that –OH and –COOH groups were present on the surface of hydrochars [37]. The peak at 2,800–3,000 cm^{-1} indicated the stretching vibrations of C–H in alkanes or carbonyls [38]. And the bands at 1,700 and 1,620 cm^{-1} were typically attributed to the C=O stretching in aldehydes and C=C stretching in aromatic ring carbon, respectively [39]. Compared with the FTIR spectra of S71T1 and S71T3, the absorption peak of S71T1 at 1,700 cm^{-1} was weakened, indicating a decrease of the C=O group in S71T1. The peak at 1,210 cm^{-1} can be attributed to the stretching vibration of C–O [30]. The peak at 1,037 cm^{-1} corresponded to the sulfonic acid group (S=O) [40], while the adsorption band of the alkyl halide groups

of C–Cl, observed in the range of 600 to 700 cm^{-1}, was relatively weakened [41].

3.5. MB adsorption experiment

3.5.1. Adsorption kinetics

Fig. 5 shows the adsorption kinetics of S71T5 and AC. The results revealed a rapid adsorption occurred within the first 10 min, which could be attributed to the abundance of active sites on the surface of S71T5 during the initial stage. Adsorption reached equilibrium within approximately 120 min. The fitting parameters of the two models are shown in Table 3, indicating the pseudo-first-order rate model was more suitable for AC adsorption (R^2 = 0.9989), while the pseudo-second-order rate model was more suitable for S71T5 adsorption (R^2 = 0.9998) [42].

3.5.2. Adsorption isotherms

As revealed in Fig. 6, the equilibrium adsorption data were analyzed by the Langmuir and Freundlich adsorption

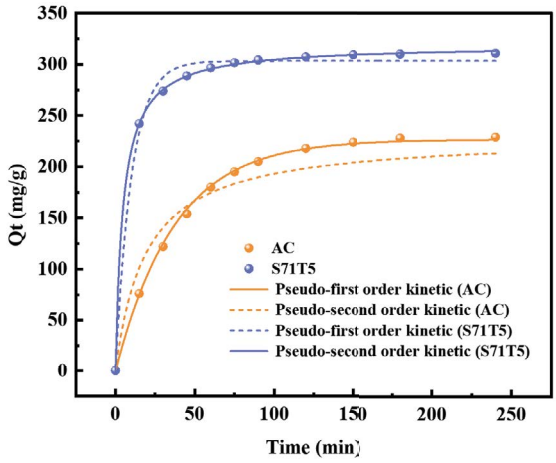

Fig. 5. Kinetic models of methylene blue adsorption on the S71T5 and activated carbon at 25°C (pH: 6.5; initial methylene blue concentration: 10 $mg{\cdot}L^{-1}$; S71T5 and activated carbon dosage: 15 mg; volume of methylene blue solution: 500 mL).

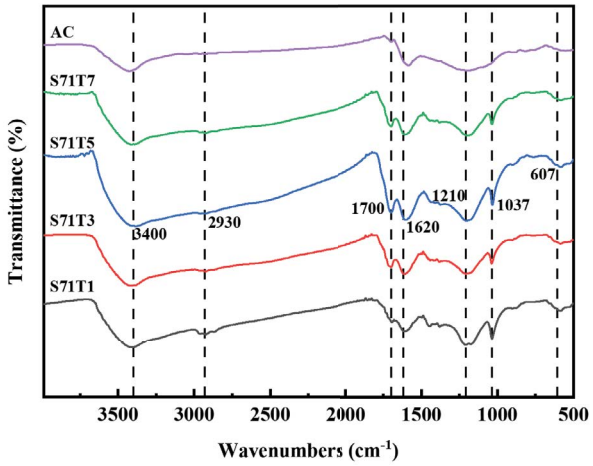

Fig. 4. Fourier-transform infrared spectra of S71T1, S71T3, S71T5, S71T7 and activated carbon.

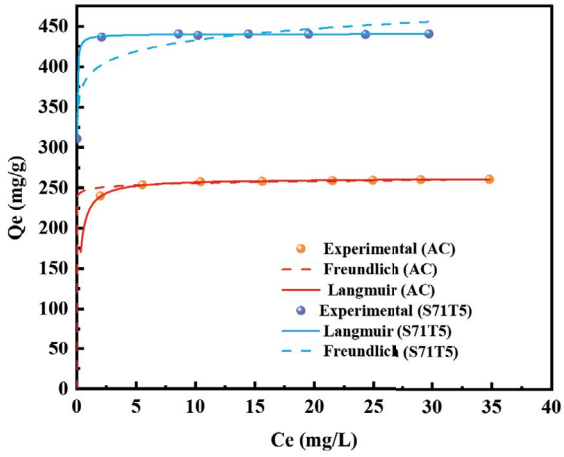

Fig. 6. Adsorption isotherms of methylene blue on the S71T5 and activated carbon.

Table 3
Kinetic constant parameters for methylene blue adsorption on the S71T5 and activated carbon

Adsorbent	Pseudo-first-order kinetic model			Pseudo-second-order kinetic model		
	k_1 (min^{-1})	Q_e ($mg{\cdot}g^{-1}$)	R^2	k_2 ($g{\cdot}mg^{-1}{\cdot}min^{-1}$)	Q_e ($mg{\cdot}g^{-1}$)	R^2
S71T5	0.0982	303.47	0.9932	0.0657	319.19	0.9998
Activated carbon	0.0268	226.60	0.9989	2.2790	217.62	0.9469

Table 4
Fitting parameters for different isotherm models

Adsorbent	Langmuir isotherm model			Freundlich isotherm model		
	Q_{max} ($mg{\cdot}g^{-1}$)	K_L ($L{\cdot}mg^{-1}$)	R^2	K_F ($L{\cdot}g^{-1}$)	n	R^2
S71T5	440.49	78.426	0.9998	388.58	21.290	0.8558
Activated carbon	261.74	1.8671	0.9985	248.02	7.3964	0.9847

isotherm models. The isotherm coefficients are displayed in Table 4. The Langmuir isotherm was found to more accurately depict the adsorption process of MB onto S71T5 and AC, as determined by the comparison of correlation coefficient (R^2) values. This indicates that the adsorption type can be classified as monolayer surface adsorption [43]. For the Langmuir isotherm, a higher adsorption equilibrium constant K_L corresponds to a stronger adsorption capacity [44]. Thus, sample S71T5 exhibited superior adsorption performance compared to AC, which was consistent with the data presented in Table 4.

4. Conclusion

The chlorinated organic waste liquids were successfully disposed of in a one-step procedure using hydrothermal carbonization assisted by NP-10. The process parameters for co-hydrothermal carbonization were determined by optimizing the NP-10/DCE mixing ratio, initial concentration of sulfuric acid, and reaction time. Under the optimized conditions, the yield of sample S71T5 increased by up to 16.49%, and the specific surface area reached up to 567.61 $m^2 \cdot g^{-1}$. The MB adsorption experiments revealed excellent adsorption performance of the sample S71T5, with a maximum adsorption capacity of 440.49 $mg \cdot g^{-1}$, surpassing that of commercial activated carbon (261.74 $mg \cdot g^{-1}$). This study provides a new and efficient technology for the treatment and management of chlorinated organic waste liquids.

Acknowledgment

This study was financially supported by the Shanghai Environmental Protection Bureau Project (Grant: 2013-6).

References

[1] E. Dobrzyńska, M. Pośniak, M. Szewczyńska, B. Buszewski, Chlorinated volatile organic compounds—old, however, actual analytical and toxicological problem, Crit. Rev. Anal. Chem., 40 (2010) 41–57.
[2] C. Dai, Y. Zhou, H. Peng, S. Huang, P. Qin, J. Zhang, Y. Yang, L. Luo, X. Zhang, Current progress in remediation of chlorinated volatile organic compounds: a review, J. Ind. Eng. Chem., 62 (2018) 106–119.
[3] F.W. Shaarani, B.H. Hameed, Ammonia-modified activated carbon for the adsorption of 2,4-dichlorophenol, Chem. Eng. J., 169 (2011) 180–185.
[4] B. Pavoni, D. Drusian, A. Giacometti, M. Zanette, Assessment of organic chlorinated compound removal from aqueous matrices by adsorption on activated carbon, Water Res., 40 (2006) 3571–3579.
[5] M. Miguet, V. Goetz, G. Plantard, Y. Jaeger, Removal of a chlorinated volatile organic compound (perchloroethylene) from aqueous phase by adsorption on activated carbon, Ind. Eng. Chem. Res., 54 (2015) 9813–9823.
[6] K. Yang, Y.J. Kong, L.Z. Huang, X.M. Hu, Catalytic elimination of chlorinated organic pollutants by emerging single-atom catalysts, Chem. Eng. J., 450 (2022) 138467, doi: 10.1016/j.cej.2022.138467.
[7] M. Mohsenzadeh, S.A. Mirbagheri, S. Sabbaghi, Degradation of 1,2-dichloroethane by photocatalysis using immobilized PAni-TiO_2 nano-photocatalyst, Environ. Sci. Pollut. Res., 26 (2019) 31328–31343.
[8] W.-G. Jeong, J.-G. Kim, K. Baek, Removal of 1,2-dichloroethane in groundwater using Fenton oxidation, J. Hazard. Mater., 428 (2022) 128253, doi: 10.1016/j.jhazmat.2022.128253.
[9] W. Zhang, P. Wei, M. Chen, L. Han, Y. Zhao, J. Yan, L. Qian, M. Gu, J. Li, Trichloroethylene dechlorination rates, pathways, and efficiencies of ZVMg/C in aqueous solution, J. Hazard. Mater., 417 (2021) 125993, doi: 10.1016/j.jhazmat.2021.125993.
[10] P. Bhatt, M.S. Kumar, S. Mudliar, T. Chakrabarti, Biodegradation of chlorinated compounds-a review, Crit. Rev. Env. Sci. Technol., 37 (2007) 165–198.
[11] V.S. Priya, L. Philip, Biodegradation of dichloromethane along with other VOCs from pharmaceutical wastewater, Appl. Biochem. Biotechnol., 169 (2013) 1197–1218.
[12] K. Yang, W. Wang, L. Li, Dechlorination of dichloromethane by a biofilter enriched with electroactive bacteria: performance, kinetics, and microbial community, Environ. Res., 215 (2022) 114247, doi: doi: 10.1016/j.envres.2022.114247.
[13] H. Matsukami, T. Kose, M. Watanabe, H. Takigami, Pilot-scale incineration of wastes with high content of chlorinated and non-halogenated organophosphorus flame retardants used as alternatives for PBDE, Sci. Total Environ., 493 (2014) 672–681.
[14] D. Wang, X. Xu, S. Chu, Q. Li, Polychlorinated naphthalenes and other chlorinated tricyclic aromatic hydrocarbons emitted from combustion of polyvinylchloride, J. Hazard. Mater., 138 (2006) 273–277.
[15] R.-D. Sun, H. Irie, T. Nishikawa, A. Nakajima, T. Watanabe, K. Hashimoto, Suppressing effect of $CaCO_3$ on the dioxins emission from poly(vinyl chloride) (PVC) incineration, Polym. Degrad. Stab., 79 (2003) 253–256.
[16] T. Hatanaka, A. Kitajima, M. Takeuchi, Role of chlorine in combustion field in formation of polychlorinated dibenzo-*p*-dioxins and dibenzofurans during waste incineration, Environ. Sci. Technol., 39 (2005) 9452–9456.
[17] Y. Shen, S. Yu, S. Ge, X. Chen, X. Ge, M. Chen, Hydrothermal carbonization of medical wastes and lignocellulosic biomass for solid fuel production from lab-scale to pilot-scale, Energy, 118 (2017) 312–323.
[18] Z. Yao, X. Ma, A new approach to transforming PVC waste into energy via combined hydrothermal carbonization and fast pyrolysis, Energy, 141 (2017) 1156–1165.
[19] X. Xu, D. Zhu, X. Wang, L. Deng, X. Fan, Z. Ding, A. Zhang, G. Xue, Y. Liu, W. Xuan, X. Li, J. Makinia, Transformation of polyvinyl chloride (PVC) into a versatile and efficient adsorbent of Cu(II) cations and Cr(VI) anions through hydrothermal treatment and sulfonation, J. Hazard. Mater., 423 (2022) 126973, doi: 10.1016/j.jhazmat.2021.126973.
[20] H.-Z. Li, Y.-N. Zhang, J.-Z. Guo, J.-Q. Lv, W.-W. Huan, B. Li, Preparation of hydrochar with high adsorption performance for methylene blue by co-hydrothermal carbonization of polyvinyl chloride and bamboo, Bioresour. Technol., 337 (2021) 125442, doi: 10.1016/j.biortech.2021.125442.
[21] Y. Wei, S. Fakudze, Y. Zhang, R. Ma, Q. Shang, J. Chen, C. Liu, Q. Chu, Co-hydrothermal carbonization of pomelo peel and PVC for production of hydrochar pellets with enhanced fuel properties and dechlorination, Energy, 239 (2022) 122350, doi: 10.1016/j.energy.2021.122350.
[22] X. Lu, X. Ma, X. Chen, Z. Yao, C. Zhang, Co-hydrothermal carbonization of polyvinyl chloride and corncob for clean solid fuel production, Bioresour. Technol., 301 (2020) 122763, doi: 10.1016/j.biortech.2020.122763.
[23] J.A. Field, R.S.-Alvarez, Biodegradability of chlorinated solvents and related chlorinated aliphatic compounds, Rev. Environ. Sci. Biotechnol., 3 (2004) 185–254.
[24] A. Grostern, E.A. Edwards, Characterization of a dehalobacter coculture that dechlorinates 1,2-dichloroethane to ethene and identification of the putative reductive dehalogenase gene, Appl. Environ. Microbiol., 75 (2009) 2684–2693.
[25] Q. Zhang, F, Wang, C. Xue, C. Wang, S. Chi, J. Zhang, Comparative toxicity of nonylphenol, nonylphenol-4-ethoxylate and nonylphenol-10-ethoxylate to wheat seedlings (*Triticum aestivum* L.), Ecotoxicol. Environ. Saf., 131 (2016) 7–13.
[26] J. Hao, W. Zhang, G. Xue, P. Rao, R. Wang, Treatment of distillation residue waste liquid from NPEOs by hydrothermal carbonization process for resource recovery, Desal. Water Treat., 125 (2018) 26–31.

[27] Q. Chen, W. Zhang, P. Rao, R. Wang, Nonylphenol ethoxylate-assisted hydrothermal preparation of carbon adsorbent from phenolic waste liquid, Desal. Water Treat., 175 (2020) 108–114.
[28] State Environmental Protection Administration of China, Water and Wastewater Monitoring and Analysis Methods, 4th ed., China Environmental Science Press, Beijing, 2002, pp. 210–213.
[29] Y. Xia, T. Yang, N. Zhu, D. Li, Z. Chen, Q. Lang, Z. Liu, W. Jiao, Enhanced adsorption of Pb(II) onto modified hydrochar: modeling and mechanism analysis, Bioresour. Technol., 288 (2019) 121593, doi: 10.1016/j.biortech.2019.121593.
[30] F.-X. Ouf, S. Bourrous, C. Vallières, J. Yon, L. Lintis, Specific surface area of combustion emitted particles: impact of primary particle diameter and organic content, J. Aerosol Sci., 137 (2019) 105436, doi: 10.1016/j.jaerosci.2019.105436.
[31] N.T.K. Thanh, N. Maclean, S. Mahiddine, Mechanisms of nucleation and growth of nanoparticles in solution, Chem. Rev., 114 (2014) 7610–7630.
[32] D.D. Eberl, J. Środoń, M. Kralik, B.E. Taylor, Z.E. Peterman, Ostwald ripening of clays and metamorphic minerals, Science, 248 (1990) 474–477.
[33] Z. Xu, R. Qi, D. Zhang, Y. Gao, M. Xiong, W. Chen, Co-hydrothermal carbonization of cotton textile waste and polyvinyl chloride waste for the production of solid fuel: interaction mechanisms and combustion behaviors, J. Cleaner Prod., 316 (2021) 128306, doi: 10.1016/j.jclepro.2021.128306.
[34] F. Ahmada, E.L. Silva, M.B.A. Varesche, Hydrothermal processing of biomass for anaerobic digestion-a review, Renewable Sustainable Energy Rev., 98 (2018) 108–124.
[35] M. Kruk, M. Jaroniec, Gas adsorption characterization of ordered organic-inorganic nanocomposite materials, Chem. Mater., 13 (2001) 3169–3183.
[36] K.S.W. Sing, Reporting physisorption data for gas/solid systems with special reference to the determination of surface area and porosity (Recommendations 1984), Pure Appl. Chem., 57 (1985) 603–619.
[37] Z. Yao, X. Ma, A new approach to transforming PVC waste into energy via combined hydrothermal carbonization and fast pyrolysis, Energy, 141 (2017) 1156–1165.
[38] B. Li, J. Guo, K. Lv, J. Fan, Adsorption of methylene blue and Cd(II) onto maleylated modified hydrochar from water, Environ. Pollut., 254 (2019) 113014, doi: 10.1016/j.envpol.2019.113014.
[39] B.-W. Lv, H. Xu, J.-Z. Guo, L.-Q. Bai, B. Li, Efficient adsorption of methylene blue on carboxylate-rich hydrochar prepared by one-step hydrothermal carbonization of bamboo and acrylic acid with ammonium persulphate, J. Hazard. Mater., 421 (2022) 126741, doi: 10.1016/j.jhazmat.2021.126741.
[40] J. Mosa, A. Durán, M. Aparicio, Sulfonic acid-functionalized hybrid organic–inorganic proton exchange membranes synthesized by sol-gel using 3-mercaptopropyl trimethoxysilane (MPTMS), J. Power Sources, 297 (2015) 208–216.
[41] N. Huang, P. Zhao, S. Ghosh, A. Fedyukhin, Co-hydrothermal carbonization of polyvinyl chloride and moist biomass to remove chlorine and inorganics for clean fuel production, Appl. Energy, 240 (2019) 882–892.
[42] Z. Duan, W. Zhang, M. Lu, Z. Shao, W. Huang, J. Li, Y. Li, J. Mo, Y. Li, C. Chen, Magnetic Fe_3O_4/activated carbon for combined adsorption and Fenton oxidation of 4-chlorophenol, Carbon, 167 (2020) 351–363.
[43] A. Zubrik, M. Matik, S. Hredzák, M. Lovás, Z. Danková, M. Kováčová, J. Briančin, Preparation of chemically activated carbon from waste biomass by single-stage and two-stage pyrolysis, J. Cleaner Prod., 143 (2017) 643–653.
[44] M.J. Ahmed, S.K. Dhedan, Equilibrium isotherms and kinetics modeling of methylene blue adsorption on agricultural wastes-based activated carbons, Fluid Phase Equilib., 317 (2012) 9–14.